JMEPEG (2015) 24:2841–2846
DOI: 10.1007/s11665-015-1588-9

1059-9495/$19.00

Fatigue Crack Growth Behavior of Nickel-base Superalloy Haynes 282 at 550-750 °C

K.A. Rozman, J.J. Kruzic, and J.A. Hawk

(Submitted June 1, 2015; published online July 7, 2015)

The fatigue crack growth rates for nickel-based superalloy Haynes 282 were measured at temperatures of 550, 650, and 750 °C using compact tension specimens with a load ratio of 0.1 and cyclic loading frequencies of 25 Hz and 0.25 Hz. Increasing the temperature from 550 to 750 °C caused the fatigue crack growth rates to increase from ~20 to 60% depending upon the applied stress intensity level. The effect of reducing the applied loading frequency increased the fatigue crack growth rates from ~20 to 70%, also depending upon the applied stress intensity range. The crack path was observed to be transgranular for the temperatures and frequencies used during fatigue crack growth rate testing. At 750 °C, there were some indications of limited intergranular cracking excursions at both loading frequencies; however, the extent of intergranular crack growth was limited and the cause is not understood at this time.

Keywords electron microscopy, fatigue crack growth rate, mechanical characterization, nickel-based superalloys

1. Introduction

Current ultra-super critical (USC) steam power plants operate at temperatures up to 610 °C with main steam inlet pressures reaching 26 MPa. This combination of temperature and pressure can yield turbine efficiencies up to 39%. To further increase steam turbine efficiency, the next generation of coal-fired advanced ultra-super-critical (A-USC) steam power plants is envisioned to push the steam inlet temperature and pressure into the range of 760 °C and 35 MPa with operational efficiencies reaching 50%. The current alloys used for high- and intermediate-pressure turbines are 9-12% Cr martensitic steel (hereafter 9% Cr steel). Other components of the turbine, including rotor casings, airfoils, and other rotating and stationary components, are also made from martensitic steel and as such they have operational temperature limits less than 620 °C (Ref 1). At temperatures above this level, 9% Cr steels experience excessive creep deformation that is unacceptable over the life of a power plant (>30 years or 2,50,000 h).

As a consequence, nickel-based superalloys are currently being investigated to replace 9% Cr steels for the high-pressure and intermediate-pressure rotors, as well as for other high-temperature critical components, in A-USC seam turbines. Haynes 282 is an alloy that possesses a combination of good high-temperature tensile strength and creep life that makes it suitable for this purpose. While tensile strength and creep performance are adequate for A-USC components (Ref 2), it is unclear if the cyclic behavior will be sufficient. Preliminary testing has shown that low-cycle fatigue at 760 °C meets minimum requirements for use as a rotor alloy (Ref 2). However, due to cyclic loads experienced during service over its lifetime, it is imperative to understand all aspects of fatigue behavior of Haynes 282 to ensure safe operation and to avoid possible catastrophic component failures.

Haynes 282 offers a unique chemistry enabling high yield strength and good creep resistance through the development of a relatively low volume fraction (~16 to 18%) of γ′ precipitates. This is in comparison to Nimonic 105, which, while having slightly better creep capability, also has a higher volume fraction of γ′ at ~36%. The lower volume fraction of γ′ for Haynes 282 provides good ductility and resistance to strain age cracking while improving fabricability and weldability relative to alloys with higher γ′ precipitate contents. Also, the aging kinetics of Haynes 282 is sluggish (Ref 3), i.e., the alloy coarsens slowly, which provides a relatively stable microstructure suitable for use at long service intervals (i.e., a creep life of at least 1,00,000 h). Oxidation resistance is reported to be similar to other low-to-

Nomenclature

R	Load ratio
P_{min}	Minimum load
P_{max}	Maximum load
ΔK	Stress intensity range
a	Crack length
W	Specimen width
B	Specimen thickness
C_p	Paris constant
m	Paris slope constant
σ	Yield strength
E	Young's modulus
T	Temperature
F	Frequency
da/dN	The crack growth rate per cycle

K.A. Rozman, ORISE, National Energy Technology Laboratory, 1450 Queen Avenue SW, Albany, OR 97321; **J.J. Kruzic**, Department of Materials Science, School of Mechanical, Industrial, and Manufacturing Engineering, Oregon State University, Corvallis, OR 97331; and **J.A. Hawk**, National Energy Technology Laboratory, 1450 Queen Avenue SW, Albany, OR 97321. Contact e-mail: jeffhawk4@comcast.net.

medium volume fraction γ′-precipitated hardened nickel-based superalloys with equivalent chromium levels (Ref 4).

Previous studies in the literature have investigated selected aspects of high-temperature mechanical behavior of Haynes 282, including low-cycle fatigue (Ref 1, 5-7), creep (Ref 1, 2, 6, 8), and tensile behavior (Ref 3-6, 9). While some fatigue crack growth testing has been done on Haynes 282 (Ref 7, 10), the literature lacks a systematic study of the fatigue crack growth resistance across the temperature regime of interest for A-USC operation. Furthermore, different cracking mechanisms may be active under varying environment and loading combinations. For example, alloys N18 (Ref 11), IN100 (Ref 12), and U720 (Ref 13) have exhibited a shift in cracking mechanism from transgranular to intergranular when the loading frequency decreased at elevated temperature in an oxygen-rich environment. Thus, it is important to know how Haynes 282 behaves at various temperatures and for various cyclic loading frequencies in order to understand the potential for fatigue mechanism change or acceleration in crack growth rates. Accordingly, the purpose of this paper is to quantify the fatigue crack growth rates and identify the crack growth mechanisms at temperatures of interest for A-USC turbine rotor service.

2. Materials and Methods

2.1 Material

A rolled plate of Haynes 282 (actual) was obtained from Haynes International in the solution-annealed condition with dimensions 333 mm × 254 mm × 35 mm. Table 1 shows the nominal and actual chemical composition for this plate of Haynes 282 (Ref 2, 6, 9). The plate was peak age heat treated in the following manner. The plate was first solutionized at >1175 °C for one hour before being cooled to near room temperature. The plate was returned to the furnace for the precipitation aging sequence starting at 1010 °C. The plate was held at this temperature for 2 h and then air cooled to below 788 °C, before reheating to 788 °C for an additional 8 h. The plate was removed from the furnace and allowed to air cool to room temperature.

The peak-aged microstructure of Haynes 282 has an ASTM grain size of 4 (~90 μm grain size) as shown in Fig. 1(a) (Ref 14). The γ′ precipitates were roughly spheroidal with a diameter of between ~20 and 50 nm as shown in Fig. 1(b) (Ref 2). No secondary or tertiary γ′ was seen in the samples tested in this research. Abundant twins are observed in the peak-aged microstructure.

The peak-aged tensile properties of Haynes 282 are shown Table 2 (Ref 2, 9). Haynes 282 has relatively constant yield strength up to around 800 °C with the yield stress only

Table 2 Typical average tensile properties of peak-aged Haynes 282 (Ref 2, 9)

Temperature, °C	0.2% Y S, MPa	UTS, MPa	Elongation, %
24	726	1196	30
204	649	1088	20
427	669	1039	27
649	633	1064	34
700	648	1016	22
750	642	887	24
816	566	652	50

Table 1 Nominal and actual chemical composition (weight percent) of Haynes 282 (Ref 2, 9)

H282	Ni	Cr	Co	Mo	Ti	Al	Fe	Mn	Si	C	B
Nominal	Bal	19.5	10	8.5	2.1	1.5	1.5	0.3	0.15	0.06	0.005
Actual	Bal	19.62	10.36	8.56	2.19	1.45	0.4	0.08	0.05	0.067	0.004

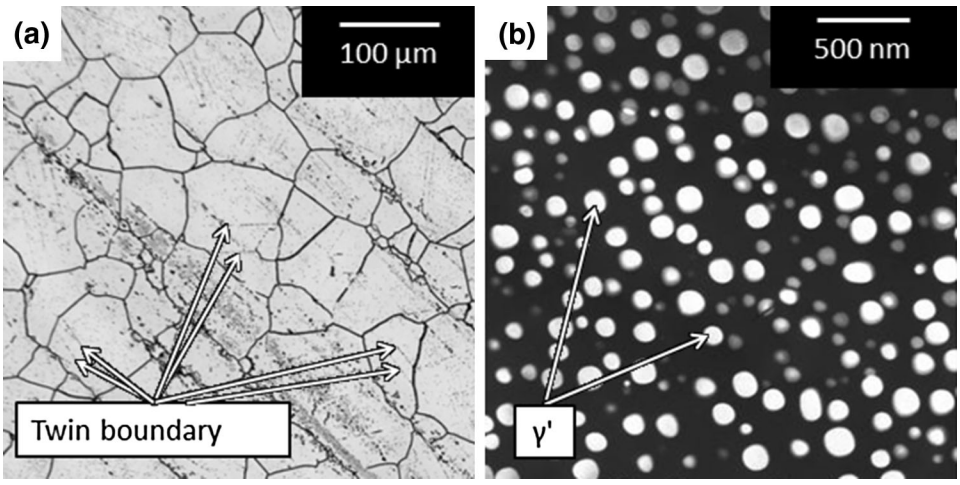

Fig. 1 (a) Microstructure of Haynes 282 in peak-aged condition with an ASTM grain size of 4. Note the abundant twin formation (Ref 14). (b) TEM dark-field image of γ′ also in peak-aged condition, from deformed material (Ref 2). The observed γ′ precipitates in Haynes 282 were measured to be between 20 and 50 nm in size

dropping by about 12% from room temperature through 760 °C.

2.2 Experimental Procedures

Fatigue crack growth experiments were conducted in general accordance with ASTM Standard E647 (Ref 15). Compact tension, C(T), specimens were machined from the peak-aged plate in the short transverse direction with the following nominal dimensions: width (W) equal to 25.4 mm and thickness (B) equal to 6.4 mm. The direct current potential drop methodology was used to monitor crack length. Current leads were attached by screw connectors at the geometric center of the sample on the top and bottom faces, while voltage leads were screwed into the front face above and below the notch. Screws were stainless steel, while the voltage leads (~0.06 mm diameter) and current leads (10 gage) were nickel. Ten amps of direct current was passed through the sample in order to measure crack length change in real time using a custom crack length calibration.

Heating the C(T) specimen was accomplished via an induction furnace coil that surrounded the C(T) specimen. Testing was performed in laboratory air. A K-type thermocouple was attached to the rear face of the C(T) specimen far away from stress zones to monitor temperature during the test. Trial tests using a sample instrumented with multiple thermocouples were used to ensure that the induction coil design provided even sample heating. Fatigue testing was performed at 550, 650, and 750 °C with temperature maintained within the C(T) specimen to ±3 °C.

A 250 kN capacity servo-hydraulic load frame was used with a 25 kN load cell. Fatigue crack growth rate tests were operated in load control. Fatigue crack growth rate testing was conducted using 25 Hz sine wave loading and 0.25 Hz triangle wave loading with a ratio of minimum to maximum load, i.e., $R = P_{min}/P_{max}$, equal to 0.1. The triangular waveform gives constant stain rates which is the more desirable loading waveform. However, the triangle waveform is unachievable at 25 Hz; therefore, the sinusoidal waveform was selected for high-frequency testing.

The C(T) specimens were first notched with a 0.6-mm-thick blade and then fatigue precracked at room temperature at a stress intensity range ($\Delta K = K_{max}$-K_{min}) of 18 MPa$\sqrt{m}$ for a minimum of 1 mm crack extension at 25 Hz. Prior to high-temperature testing, samples were held at the testing temperature for 24 h. During this 24-h hold period, the C(T) specimens were cycled below the threshold crack growth rate (ΔK of ~2 to 3 MPa$\sqrt{m}$). This step was performed to stabilize the system and thus minimize voltage drift, thermocouple effects, and temperature fluctuations. Fatigue crack growth rate, da/dN, data were gathered in two steps. First, load shedding tests were performed using a load shedding constant of -0.24 mm^{-1} from ~16 MPa$\sqrt{m} > \Delta K >$ 6 MPa$\sqrt{m}$ for crack lengths in the range of ~9 mm $< a <$ 14 mm. After load shedding experiments were completed, constant load tests were performed with an initial ΔK_i = 10 MPa$\sqrt{m}$ until the crack length reached an a/W ratio of 0.8 ($a \sim 20$ mm).

Experiments were performed using a load shedding constant according to the ASTM Standard E647 of -0.08 mm^{-1} at both 550 and 650 °C from 8 MPa$\sqrt{m} < \Delta K <$ 16 MPa$\sqrt{m}$ to compare with the more aggressive load shedding constant. Data showed overlapping fatigue crack growth rates between the two load shedding constants. Load shedding experiments were not done at 750 °C due to concerns about clevis and loading pin creep during long-term experiments. To precrack the specimen intended for constant load amplitude testing at 750 °C, the load shedding procedure previously described was also used, but with a temperature of 650 °C. Subsequent constant load testing commenced with an initial ΔK_i = 10 MPa$\sqrt{m}$ until crack length reached an a/W ratio of 0.8 ($a \sim 20$ mm) with testing temperature at 750 °C.

The fracture surfaces were investigated using a scanning electron microscope (FEI, Inspect F) in secondary electron imaging mode. In order to estimate the applied stress intensity range representative of the image, the crack length location of each image was recorded and correlated to an applied ΔK from the measured data.

3. Results and Discussion

3.1 Fatigue Crack Growth Rates

Figure 2 shows the measured da/dN values as a function of the applied ΔK for Haynes 282 at 550, 650, and 750 °C. Figure 2(a) shows the crack growth rate curves at a loading

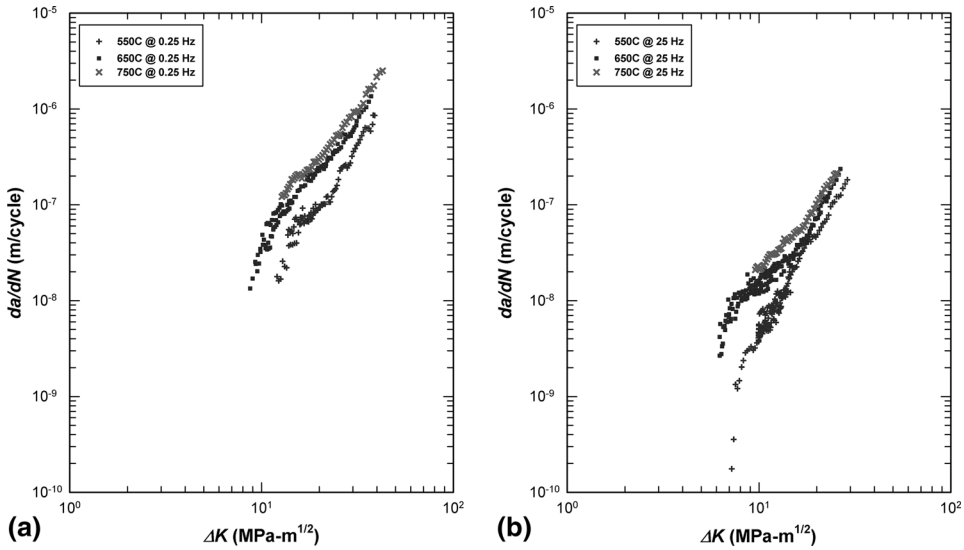

Fig. 2 Fatigue crack growth rates of Haynes 282 with a load ratio of 0.1. Temperature indicated on plot. (a) At 0.25 Hz with triangular waveform and (b) at 25 Hz with sinusoidal waveform

frequency of 0.25 Hz, while Fig. 2(b) shows them at a loading frequency of 25 Hz. The effect of increasing temperature on fatigue crack growth rate was to increase *da/dN* at a given applied ΔK. The effect of lowering the cycle frequency was to increase the *da/dN* at a given applied ΔK as well. The frequency effect was larger at 650 and 750 °C.

Buckson and Ojo examined the fatigue crack growth properties of Haynes 282 at 600 °C using both 0.05 and 15 Hz sine waveforms. Their data at 0.05 Hz fell in well with the data for the present study at 0.25 Hz shown in Fig. 2(b). Buckson and Ojo's 15 Hz data and the present 25 Hz data also correlate well over most of their reported ΔK values; however, at low ΔK they reported a fatigue threshold at around 10 MPa√m that was not observed in the present study. However, it is important to note that their microstructure contained large primary γ' precipitates that may contribute to mechanical property differences (Ref 14). Ismonov et al. (Ref 10) reported some crack growth data at 649 and 760 °C; however, they did not report the loading frequency nor provided many experimental details. Their results show considerable overlap with the present results at 0.25 Hz suggesting that they used a relatively low loading frequency.

Paris and Erdogan (Ref 16) observed a power law relationship between applied ΔK and *da/dN*. This relationship is empirical and generally assumed true over decades of fatigue crack growth rate data for most alloys and materials. The power law relationship is typically referred to as the 'Paris law' and is formulated in Eq 1:

$$da/dN = C_p \Delta K^m, \quad \text{(Eq 1)}$$

where *da/dN* is the crack growth rate per cycle, C_p is the Paris coefficient, m is the Paris exponent, and ΔK is the stress intensity range.

The scaling constants for the Paris law (C and m) are dependent on the microstructure, environment, temperature, and load ratio, R. Fitting fatigue crack growth data to the Paris law allows quantification of changes in the fatigue crack growth data due to temperature or cyclic loading frequency changes.

The fatigue data in Fig. 2 were subsequently fit to the Paris law. This information is presented in Table 3. For 25 Hz loading frequency, the crack growth rate curves at 650 and 750 °C showed a change in slope in the Paris region around ΔK = 17 MPa√m (Fig. 2b). This slope change is also consistent with the results of other researchers (Ref 10). Accordingly, the Paris constants were determined separately for ΔK above and below 17 MPa√m for 750 and 650 °C with 2 MPa√m overlap. Increasing the temperature had minor effects on the Paris exponent (m) and did not show a clear monotonic trend. In contrast, by reducing the loading frequency, the Paris exponent always decreased at the high stress intensity ranges ($\Delta K > 17$ MPa√m), by 18, 40, and 24% for 550, 650, and 750 °C, respectively.

Table 3 Paris constants for each test temperature and frequency

Temperature, °C	Frequency, Hz	ΔK, MPa√m	C_p	m
550	25	10-29	1.42×10^{-12}	3.50
650	25	10-18	4.38×10^{-10}	1.58
650	25	16-24	9.01×10^{-13}	3.78
750	25	10-18	2.51×10^{-10}	1.94
750	25	16-25	7.37×10^{-12}	3.19
550	0.25	12-39	1.97×10^{-11}	2.87
650	0.25	10-34	2.60×10^{-10}	2.28
750	0.25	13-41	2.50×10^{-10}	2.41

Paris constants for 650 and 750 °C split at ΔK = 17 MPa√m

3.2 Fractography

Typical polycrystalline metallic fracture surfaces exhibit either transgranular or intergranular growth. Intergranular crack growth occurs when the crack grows along grain boundaries, revealing grain facets on the fracture surface. Transgranular crack growth occurs through the grains, leaving a more planar fracture surface.

Transgranular crack growth occurs in two distinct stages (Ref 17). During the first stage, only one dislocation slip system is active, leaving a zigzag-like pattern on the fracture surface. During stage two, multiple dislocation slip systems are active,

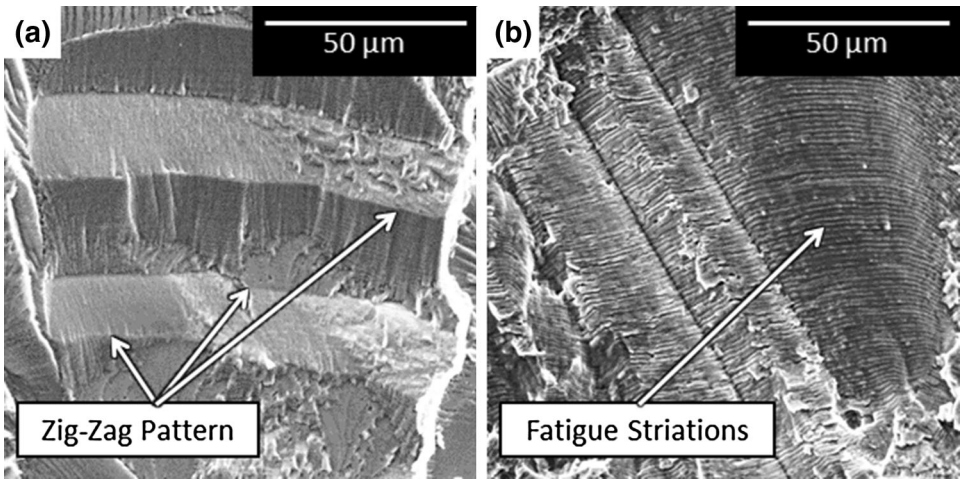

Fig. 3 Fracture surfaces of Haynes 282 at various temperatures and stress intensity ranges. Crack growth direction is from bottom to top for all images (a and b). Both images are scaled equivalently. (a) Typical zigzag-type stage-one crack growth with experimental conditions: $\Delta K \sim 14$ MPa√m, T = 550 °C, and f = 0.25 Hz. (b) Typical fatigue striation stage-two crack growth with experimental conditions: $\Delta K \sim 41$ MPa√m, T = 550 °C, and f = 0.25 Hz

and the crack grows by a blunting and re-sharpening mechanism. Distinct fractographic features of stage-two growth include fatigue striations and the absence of the stage-one zigzag-like pattern.

Post failure analysis of the fatigue fracture surfaces reveals typical transgranular features under all experimental conditions (550 °C $< T <$ 750 °C; 0.25 Hz $< f <$ 25 Hz). Stage-one crack growth produced the zigzag-like pattern (Fig. 3a) and was observed independent of loading frequency or test temperature. Stage-one crack growth persisted until a ΔK of 14 MPa√m was reached for $T \leq$ 650 °C and was independent of loading frequency. After a ΔK of 14 MPa√m, typical stage-two crack growth was observed. During this stage of crack growth fatigue striations (Fig. 3b) appeared. At 750 °C, the appearance of fatigue striations was delayed until a ΔK of 20 MPa√m and was also independent of loading frequency.

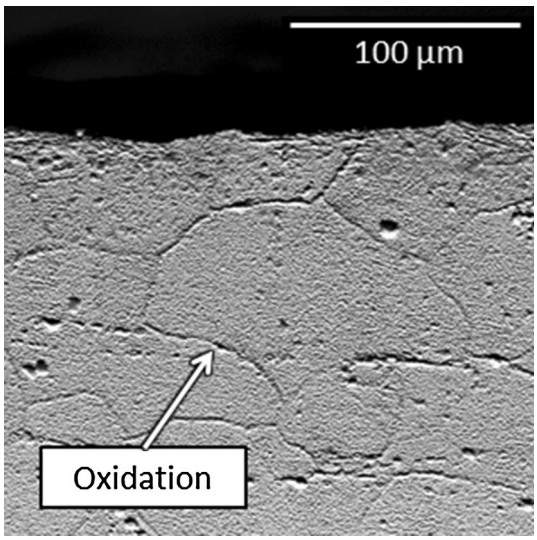

Fig. 4 Transverse orientation of C(T) specimen showing transgranular crack path for this fatigue crack growth rate test. Oxidation reveals grain boundaries. Experimental conditions: $\Delta K \sim 10$ MPa√m, $T = 650$ °C, and $f = 25$ Hz

Orienting the C(T) specimen on its side, the crack profile may be observed. The crack profile was very smooth (Fig. 4) indicating that crack closure and bridging are not anticipated to be significant in this alloy. Oxidation in air during the fatigue crack growth test revealed the grain boundaries. The crack path is observed to traverse through grains (rather than follow the grain boundaries), thereby providing additional evidence of transgranular crack growth.

Other notable features observed from fractographic inspection include randomly oriented secondary cracking observed throughout the entirety of test temperatures and loading frequencies suggesting the occasional bifurcation of the crack front. Unique to the fracture surface at 750 °C, intergranular fracture surface features were dispersed and isolated. At 25 Hz, these intergranular crack path excursions were limited to a single grain. Typical observations included pull-out of the corners of a single grain (not shown) or grain boundary cavitation between adjacent grains (Fig. 5a). The intergranular features at 25 Hz loading frequency ceased for $\Delta K > 11$ MPa√m.

At 0.25 Hz loading frequency, the occasional intergranular features were present at all applied ΔK values. At the lower ΔK values, the area of the intergranular features was sometimes larger including clusters of multiple grains (Fig. 5b). In contrast, at higher ΔK values the intergranular feature effects were observed to be isolated to single grains.

While an increase in testing temperature increased the crack growth rate, *da/dN*, no significant fractographic changes were noted, suggesting a change in the deformation mechanism or mode of fracture at, or below, 650 °C. While some intergranular features could be found at 750 °C, these features were rare and isolated and did not suggest a wholesale change in cracking mechanism. This observation is consistent with the very modest increase in crack growth rates observed between 650 and 750 °C at both cyclic loading frequencies.

4. Conclusion

In summary, this study has evaluated the fatigue crack growth rates of Haynes 282 at 550, 650, and 750 °C for cyclic

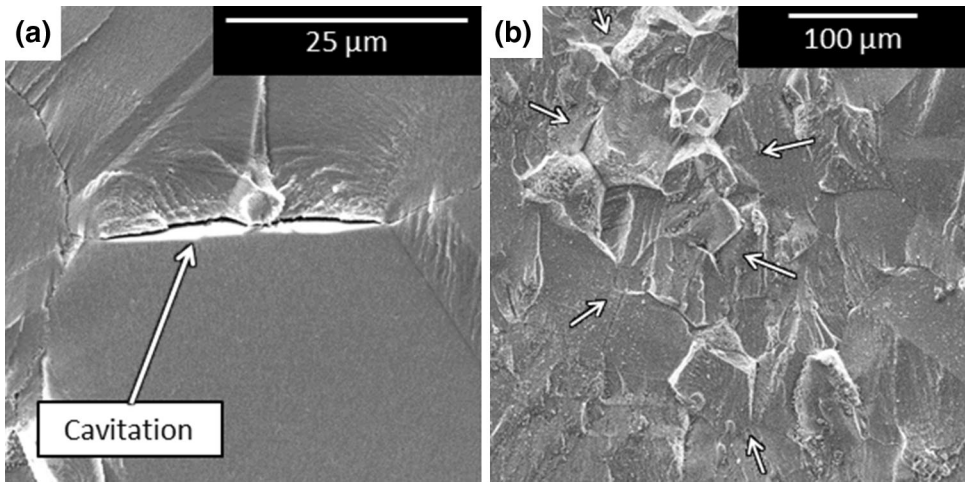

Fig. 5 SEM micrographs showing observed intergranular features dispersed on fracture surface tested at 750 °C. Crack growth direction is from bottom to top of both images. (a) Example of grain boundary (GB) cavitation with experimental conditions of $T = 750$ °C, $f = 25$ Hz, and $\Delta K \sim 9$ MPa√m. (b) Example of a limited intergranular (IG) cluster with experimental conditions of $T = 750$ °C, $f = 0.25$ Hz, and $\Delta K \sim 14$ MPa√m

frequencies of 25 and 0.25 Hz. Based on those results, the following conclusions are made:

- Increasing the testing temperature showed a corresponding increase in fatigue crack growth rates.
- Decreasing the testing frequency showed a corresponding increase in fatigue crack growth rates.
- Fractography revealed that failure occurred transgranularly at all temperatures with very little intergranular fracture even at 750 °C.

With no observed change in fracture mode either due to increasing temperatures or decreasing frequencies, it is expected that the fatigue performance of Haynes 282 will be robust and predictable up to the target peak temperature for A-USC steam turbines. However, problems may arise with hold times and creep fatigue loading; thus, further investigation is strongly suggested before use of Haynes 282 in critical components at elevated temperatures.

Acknowledgment

This research was supported in part by an appointment to the U.S. Department of Energy (DOE) Postgraduate Research Program at the National Energy Technology Laboratory administered by the Oak Ridge Institute for Science and Education. The authors would also like to thank Dr. Rawley Greene for experimental support and technical programming.

Disclaimer

References

1. R. Viswanathan, J.F. Henry, J. Tanzosh, G. Stanko, J. Shingledecker, B. Vitalis, and R. Purgert, U.S. Program on Materials Technology for Ultra-Supercritical Coal Power Plants, *J. Mater. Eng. Perfor.*, 2013, **22**(10), p 2904–2915. doi:10.1007/s11665-013-0717-6
2. R. Viswanathan, J.A. Hawk, R.C. Schwant, D. Saha, T. Totemeier, S. Goodstine, M. Mcnally, and D.B. Allen, *Steam Turbine Materials for Ultrasupercritical Coal Power Plants*, Final Technical Report, DOE DE-FC26-05NT42442/OAQDA-OCDO 05-02(B), 2009, 535 p
3. L.M. Pike, Long Term Thermal Exposure of HAYNES 282 Alloy. *Superalloy 718 and Derivatives*, 2012, p 645–660. Retrieved from http://onlinelibrary.wiley.com/doi/10.1002/9781118495223.ch50/summary
4. L.M. Pike and S.K. Srivastava Oxidation Behavior of Wrought Gamma-Prime Strengthened Alloys. *Materials Science Forum*. *595–598*, 2008, p 661–671. doi:10.4028/www.scientific.net/MSF.595-598.661
5. L.M. Pike, Low-Cycle Fatigue Behavior of HAYNES, in *Turbo Expo 2007*, Vol. 5, 2007, p 161–169. doi:10.1115/GT2007-28267
6. Haynes® International *Haynes*® 282® Alloy, 2006. Retrieved from http://www.haynesintl.com/pdf/h3173.pdf. Accessed 1 Jan 2015
7. R.A. Buckson and O.A. Ojo, Cyclic Deformation Characteristics and Fatigue Crack Growth Behaviour of a Newly Developed Aerospace Superalloy Haynes 282, *Mater. Sci. Eng. A*, 2012, **555**, p 63–70. doi:10.1016/j.msea.2012.06.034
8. C.J. Boehlert and S.C. Longanbach, A Comparison of the Microstructure and Creep Behavior of Cold Rolled HAYNES® 230 alloy^{tm} and HAYNES® 282 alloy^{tm}, *Mater. Sci. Eng. A*, 2011, **528**(15), p 4888–4898. doi:10.1016/j.msea.2011.03.019
9. L.M. Pike, ASME Turbo Expo 2006: Power for Land, Sea and Air, in *Haynes 282 Alloy—A New Wrought Superalloy Designed for Improved Creep Strength and Fabricabilty, GT2006-91204,* Barcelona, 2006, p 1–9
10. S. Ismonov, A. Loghin, T. Hanlon, and C. Shen, Application of Crack Tip Plasticity Based Fatigue Model on High Temperature Alloy HAYNES® 282®, *Int. J. Fatigue*, 2015, **70**, p 146–153. doi:10.1016/j.ijfatigue.2014.08.015
11. S. Everitt, R. Jiang, N. Gao, M.J. Starink, J.W. Brooks, and P.A. Reed, Comparison of Fatigue Crack Propagation Behaviour in Two Gas Turbine Disc Alloys Under Creep–Fatigue Conditions: Evaluating Microstructure, Environment and Temperature Effects, *Mater. Sci. Technol.*, 2013, **29**(7), p 781–787. doi:10.1179/1743284713Y.0000000229
12. B.S. Adair, W.S. Johnson, S.D. Antolovich, and A. Staroselsky, Identification of Fatigue Crack Growth Mechanisms in IN100 Superalloy as a Function of Temperature and Frequency, *Fatigue Fract. Eng. Mater. Struct.*, 2013, **36**(3), p 217–227. doi:10.1111/j.1460-2695.2012.01715.x
13. G. Onofrio, G.A. Osinkolu, and M. Marchionni, Effects of Loading Waveform on Fatigue Crack Growth of Udimet 720 Li Superalloy, *Int. J. Fatigue*, 2004, **26**(3), p 203–209. doi:10.1016/S0142-1123(03)00170-1
14. K.A. Rozman *Characterization of High Temperature Fatigue Mechanisms in Haynes 282 Nickel Based Superalloy.* Doctoral dissertation, Oregon State University, Corvallis, 2014
15. ASTM Standard E647 – 11: *Standard Test Method for Measurement of Fatigue Crack Growth Rates*. ASTM International, West Conshohocken, PA, 2011. doi:10.1520/E0647-13AE01, www.astm.org
16. P. Paris and F. Erdogan, A Critical Analysis of Crack Propagation Laws, *J. Fluids Eng.*, 1963, **85**(4), p 528–533. doi:10.1115/1.3656900
17. S. Suresh, *Fatigue of Materials*, 2nd ed., Cambridge University Press, Cambridge, 2004